Waste-derived Fe_3O_4/ZnO composite for advanced Fenton-like wastewater treatment

Oman Zuas[1,*], Nuryatini Hamim[2], Nurhani Aryana[2], Wuwus Ardiatna[3], Elvina Trivida[4], Suherlan Dayat Sudayat[3], Andi Suhandi[5], Toto Sudiro[5], Fakhzah Aliifatudz Dzakirah[6]

[1]*Research Centre for Catalysis, National Research and Innovation Agency, Republic of Indonesia, Building 456, K.S.T-BJ. Habibie, Indonesia*

[2]*Research Centre for Molecular Chemistry, National Research and Innovation Agency, Republic of Indonesia, Building 452, K.S.T-BJ. Habibie, Indonesia*

[3]*Research Centre for Equipment Manufacturing Technology, National Research and Innovation Agency, Republic of Indonesia, Building 720, K.S.T-BJ. Habibie, Indonesia*

[4]*Research Centre for Electrical Technology, National Research and Innovation Agency, Republic of Indonesia, K.S.T-BJ. Habibie, Indonesia*

[5]*Research Centre for Energy Materials, National Research and Innovation Agency, Republic of Indonesia, Building 440-442, K.S.T-BJ. Habibie, Indonesia*

[6]*Chemistry Department, Faculty of Natural Science, Universitas Negeri Malang, Semarang Street No.5, 65145, East Java, Indonesia*

Received 15 July 2025; received in revised form 9 December 2025; accepted 25 January 2026

Abstract

This study presents a novel and sustainable precipitation method for synthesis of Fe_3O_4/ZnO composite powder directly from corrugated galvanised iron (CGI) waste, addressing gaps in waste-derived catalysts for advanced oxidation processes. XRD characterisation revealed that the Fe_3O_4/ZnO powder contains the dominant Fe_3O_4 (magnetite) crystalline phase with minor amount of ZnO phase. FTIR spectroscopy verified Fe–O (571 cm^{-1}) and Zn–O (450–500 cm^{-1}) bonds, while XPS confirmed coexistence of Fe^{2+}/Fe^{3+} (710/724 eV) and Zn^{2+} (1022/1045 eV) cations essential for redox cycling. The composite powder showed irregular, agglomerated morphology (SEM/TEM, 20–150 nm particles), mesoporosity (BET 22.69 m^2/g, Type IV isotherm) and superparamagnetic properties (Ms ≈ 51 emu/g). Preliminary Fenton-like tests achieved 85.47% methylene blue (MB) degradation in 60 min (first-order reaction, k = 0.024 min^{-1}) via $^{\bullet}OH$ generation, with >93% efficiency over 4 reuse cycles and facile magnetic separation. This reinforces waste valorisation for sustainable wastewater treatment, demonstrating a synergistic effect at the Fe_3O_4/ZnO interface for scalable environmental remediation.

***Keywords**: precipitation, Fe_3O_4/ZnO, porous material, structural characterisation, catalytic properties*

I. Introduction

The rapid increase in industrial activity and population growth has intensified global waste generation, including substantial quantities of corrugated galvanised iron (CGI) roofing waste [1]. Despite containing significant amounts of iron and zinc, CGI is commonly discarded, overlooking its potential as a precursor for functional materials. Converting CGI waste into value-added products aligns with circular economy principles [2], while simultaneously mitigating environmental pressure associated with metal-rich solid waste, offering a sustainable route for resource recovery. Previous studies highlight that industrial residues can serve as low-cost sources for iron- and zinc-based oxides in catalysis and environmental remediation [3,4].

Despite these promising routes, direct conversion of CGI waste into Fe_3O_4/ZnO composites for heterogeneous Fenton-like catalysis remains poorly

*Corresponding author: tel: +62 812 8853 0160
e-mail: *oman003@brin.go.id*

explored, representing a critical gap in sustainable materials design. No prior study has systematically synthesised Fe_3O_4/ZnO composites directly from CGI waste, nor evaluated their structural, surface and magnetic characteristics in relation to catalytic performance, leaving an opportunity to establish structure–function relationships that govern redox behaviour, reactive oxygen species (ROS) production and catalyst reusability.

Fe_3O_4-based materials are well recognised for their catalytic efficiency in heterogeneous Fenton-like processes due to their mixed Fe^{2+}/Fe^{3+} redox cycling, enabling continuous generation of hydroxyl radicals ($^{\bullet}OH$) from hydrogen peroxide [5–8]. Besides, the magnetic properties of Fe_3O_4 enable facile separation and reuse of the catalyst [5,8].

ZnO, in turn, is a chemically stable, relatively non-toxic semiconductor with diverse functionalities [9–13]. While ZnO is often applied in photocatalysis [10,14] its role in Fenton-like systems is functionally significant, promoting electron transfer processes that accelerate $Fe^{3+} \rightarrow Fe^{2+}$ regeneration, reducing Fe^{3+} accumulation at the catalytic interface, and enhancing $^{\bullet}OH$ production [4,15,16]. These effects establish a synergistic Fe_3O_4/ZnO interface, where ZnO not only contributes structurally but also functionally to sustaining the redox cycle. In this context, "advanced" Fenton-like treatment refers to heterogeneous catalytic systems capable of operating under broader pH ranges, minimising secondary waste, enabling magnetic recovery and achieving higher reactive oxygen species (ROS) generation efficiency compared to classical homogeneous Fenton processes [4–7,16,17]. These characteristics make advanced Fenton-like catalysts practical for real wastewater conditions, where strict pH adjustment is often impractical.

Unlike previous studies that utilised synthetic precursors [5,7,16] or mixed industrial wastes [3,4], this work employs CGI waste as the sole metal source, enabling a sustainable and streamlined synthesis approach. Accordingly, this study develops a Fe_3O_4/ZnO composite powder through a simple precipitation method using CGI waste as the sole metal source. Comprehensive characterisation and evaluation of its Fenton-like degradation performance were conducted, highlighting the potential of industrial waste valorisation for producing functional, magnetically recoverable catalysts for sustainable wastewater treatment and scalable environmental applications.

II. Experimental

2.1. Synthesis of Fe_3O_4/ZnO composite

Fe_3O_4/ZnO composite powder was prepared from corrugated galvanised iron (CGI) roofing sheet waste, collected from a local construction site. According to literature reports, CGI typically consists of ~99.5% Fe (steel substrate) and ~0.5–1.2% Zn (coating layer) [18]. By considering the upper-limit of the Zn content (1.2%), the effective composition corresponds to ~98.8% Fe and 1.2% Zn, yielding an Fe:Zn mass ratio of approximately 83:1 in the precursor material. This highly Fe-rich composition inherently favours the formation of Fe_3O_4 as the dominant crystalline phase, with ZnO expected only as a minor accompanying phase. All chemicals are used in this study without further purification, including nitric acid (HNO_3, 65%, Sigma-Aldrich), sodium hydroxide (NaOH, ~98%, Merck), hydrogen peroxide (H_2O_2, 30%, Sigma-Aldrich) and methylene blue (MB, analytical grade, Sigma-Aldrich). Double-deionized water was employed throughout all experiments.

CGI waste pieces with minimal corrosion were selected and mechanically cleaned before processing. The cleaned pieces (~0.5 × 0.5 cm) were dissolved in 65% HNO_3 (5 g CGI per 20 ml acid) at room temperature to release Fe and Zn ions into solution. Following dissolution, the obtained solution was filtered to remove insoluble residues and diluted to 200 ml. A 100 ml aliquot was titrated with 2.5 M NaOH to pH 11 under constant stirring at 50–60 °C for 2 h to induce co-precipitation of Fe and Zn species. The resulting black precipitate was separated via decantation and attracted to a permanent magnet. It was subsequently rinsed with double-deionised water until the pH became neutral (pH = 7) and no chloride ions (Cl^-) were detected, as confirmed using a 0.1 mM $AgNO_3$ solution. Given that HNO_3 was used during dissolution, nitrate ions were initially present. However, their high solubility under alkaline conditions and the subsequent washing steps greatly reduced the likelihood of their retention in the solid. FTIR and XPS were further employed to verify this. The precipitate was further washed with 100 ml of ethanol and dried in an oven at 80 °C for 12 h. The synthesised Fe_3O_4/ZnO composite powder was stored in a sealed container for further use.

2.2. Characterisation

The Fe_3O_4/ZnO composite powder was characterised using X-ray diffraction (XRD, Rigaku SmartLab X-ray diffractometer) to analyse the crystal structure within a 2θ range of 20–70°. Fourier-transform infrared spectroscopy (FTIR, Bruker Invenio S FTIR spectrometer) was performed to identify functional groups in the range of 4000–400 cm^{-1}. The absorption spectra of the samples were recorded using a UV-Vis spectrophotometer (Shimadzu 2450, Japan) to determine absorbance within the wavelength range of 200–800 nm. Morphology and elemental composition were determined by scanning electron microscopy with energy-dispersive X-ray spectroscopy (SEM-EDX,

JEOL JSM-IT200). Transmission electron microscopy (TEM, Tecnai G2 20 S-TWIN) was used to examine particle nanostructure. X-ray photoelectron spectroscopy (XPS, Kratos Analytical Axis Supra+ system) equipped with ESCApe software, was used to determine the elemental composition and surface chemical states, including any potential incorporation of nitrogen species into the Fe_3O_4/ZnO composite. Magnetic properties were measured at room temperature using a vibrating sample magnetometer (Oxford Instruments 1.2H VSM) within a magnetic field range of -1 to 1 T. The specific surface area and pore characteristics were analysed using Brunauer-Emmett-Teller (BET) N_2 adsorption-desorption method with a Quantachrome NovaWin automated surface area and pore size analyser, following degassing at 200 °C.

2.3. Fenton-like catalytic activity evaluation

The Fenton-like catalytic activity of the Fe_3O_4/ZnO composite was evaluated through the degradation of MB in the presence of H_2O_2. In a typical experiment, 50 mg of the Fe_3O_4/ZnO composite was added to 100 ml of a 10 ppm MB solution. The suspension was continuously stirred at 250 rpm in the dark at room temperature for 60 min to reach adsorption-desorption equilibrium. Subsequently, 150 µl of 30% H_2O_2 was added to initiate the Fenton-like reaction. Notably, the entire degradation process was performed under light-excluded conditions to eliminate any photocatalytic effects and ensure that the degradation proceeded exclusively via the Fenton-like catalytic pathway. At specific time intervals (0, 10, 20, 30, 40, 50 and 60 min), aliquots were collected, and the catalyst was immediately separated using an external magnet. The supernatant was centrifuged at 6000 rpm for 4 min and recorded using a UV-Vis spectrophotometer (PerkinElmer Lambda 35 UV/Vis spectrophotometer). The degradation efficiency (D) was calculated using the following equation [19]:

$$D = \frac{C_0 - C_t}{C_0} \times 100 \quad (1)$$

The MB concentration at each time interval was used to determine the degradation kinetics based on the first-order (Eq. 2) and second-order models (Eq. 3) [20,21]:

$$\ln \frac{C_0}{C_t} = -kt \quad (2)$$

$$\frac{1}{C_0} - \frac{1}{C_t} = kt \quad (3)$$

where C_0 is the initial concentration of MB (ppm), C_t is the concentration of MB (ppm) at a given time (t), and k is the reaction rate constant. For the reusability test, the recovered catalyst was washed several times (e.g. three times) with double-distilled water, dried at 60 °C for 12 h, and reused under the same conditions for subsequent degradation cycles.

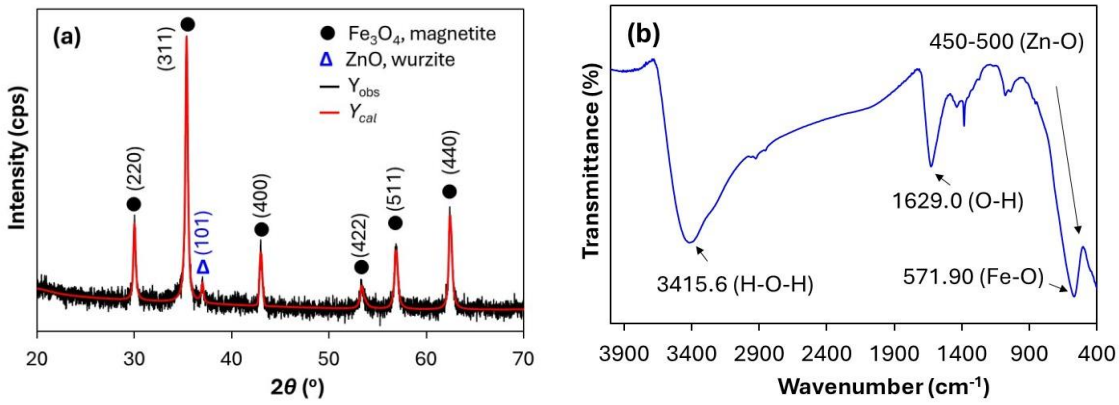

Figure 1. XRD pattern (a) and FTIR spectrum (b) of the synthesised Fe_3O_4/ZnO composite powder, showing the phase composition and characteristic functional groups

III. Results and discussion

3.1. Characterisation results

The crystal structure and phase composition of the synthesised Fe_3O_4/ZnO composite were analysed by XRD (Fig. 1a). The XRD pattern confirms the predominant presence of the Fe_3O_4 phase, with distinct characteristic peaks at 2θ values of 29.98°, 35.34°, 42.93°, 53.31°, 56.83° and 62.41°. These peaks are well-matched with the (220), (311), (400), (422), (511) and (440) crystal planes of cubic spinel-structured magnetite (JCPDS No. 19-0629) [22]. Importantly, the presence of ZnO is also detectable, indicated by peak at 36.99°, corresponding to the (101) plane of hexagonal wurtzite ZnO (JCPDS No. 36–1451) [23]. The coexistence of Fe_3O_4 and ZnO phases in the composite, without the formation of any new phases,

is significant as it preserves the intrinsic catalytic functionalities of both components. A qualitative intensity-based estimation further supports this phase distribution, where Fe_3O_4 accounts for approximately 97.2% of the total integrated peak intensity compared to only 2.8% for ZnO, reinforcing Fe_3O_4 as the overwhelmingly dominant crystalline phase. Nevertheless, precise phase quantification would require formal refinement.

The FTIR spectrum (Fig. 1b) supports the XRD findings by confirming characteristic bonds for both Fe_3O_4 and ZnO phases. A prominent Fe–O stretching mode appears at 571.9 cm^{-1}, typical of Fe_3O_4 structure [24,25]. Weaker bands in the 450–500 cm^{-1} range correspond to Zn–O stretching vibration of ZnO [26]. Furthermore, although a weak band appears near 1384 cm^{-1}, it cannot be assigned to nitrate because it lacks the required accompanying absorption in the 820–860 cm^{-1} region; thus, no absorption features characteristic of nitrate (~1300–1500 cm^{-1} and ~700–860 cm^{-1}) or nitrite (~1250–1320 cm^{-1} and ~820–900 cm^{-1}) [27–29] were detected, confirming that nitrogen-containing species were not incorporated into the final composite powder. Additionally, broad absorbance bands at 1629.0 and 3415.6 cm^{-1} relate to H–O–H deformation and O–H stretching, respectively, indicating the adsorption of water molecules or hydroxyl groups on the composite surface [30].

SEM analysis (Figs. 2a,b) reveals that the Fe_3O_4/ZnO composite particles are nearly spherical yet polydispersed, exhibiting a rough and heterogeneous surface morphology. At lower magnification (10,000×, Fig. 2a), dense and irregular particle agglomerations are visible. At higher magnification (20,000×, Fig. 2b), morphology clarifies, showing a more uniform agglomerate structure. This observation aligns with previous reports describing Fe-doped ZnO nanomaterials with similar morphology [31]. The inset in Fig. 2b shows particles ranging from sub-micrometer to micrometer scale. Agglomeration likely results from strong magnetic interactions among Fe_3O_4 nanoparticles, consistent with prior observations in Fe_3O_4-AgBr composites [32].

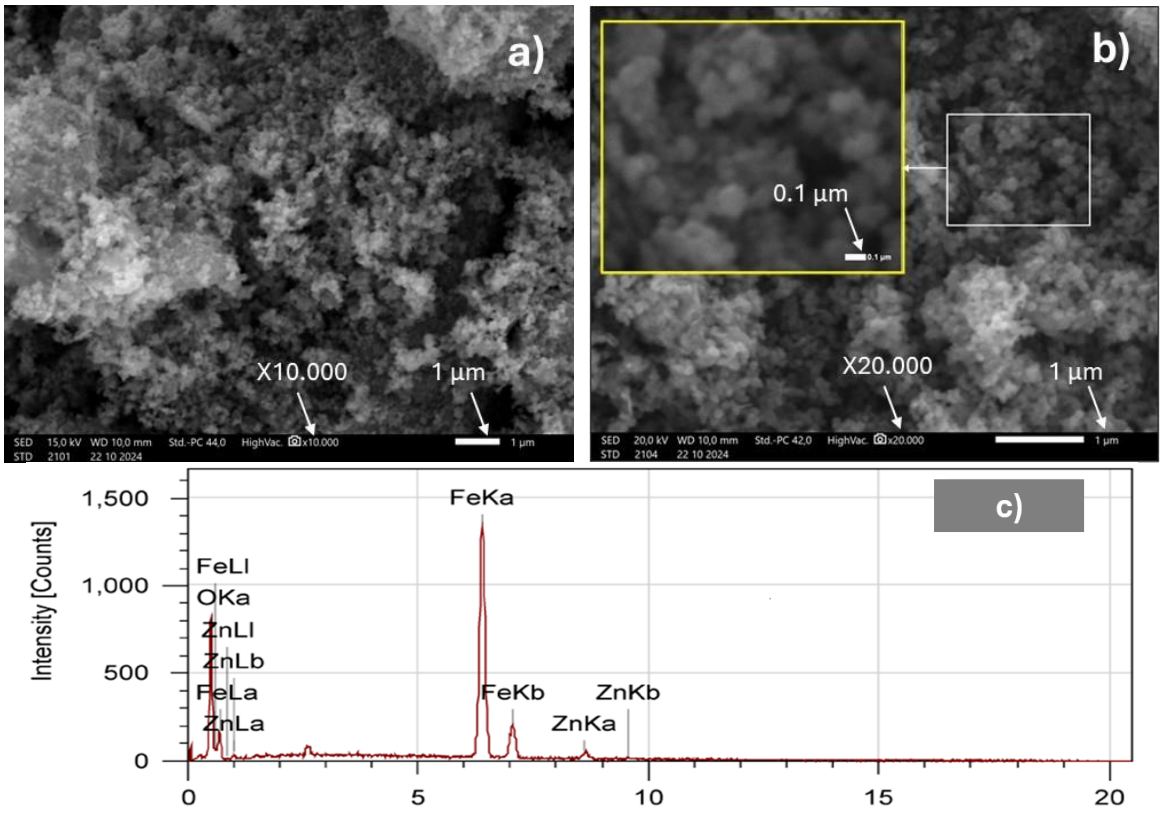

Figure 2. SEM images of the Fe_3O_4/ZnO composite at different magnifications (a, b) and EDX spectrum taken from the area within the box in Figure 2b (c), confirming the presence of Fe and Zn elements

Elemental composition analysis by EDX spectroscopy (Fig. 2c) identifies Fe, O and Zn in the composite powder. The Fe and O peak intensities dominate those of Zn, quantitatively indicating Fe_3O_4 as the primary phase and ZnO as the minor phase. This dominance relates to the raw material, corrugated galvanised iron waste, which is rich in iron with limited zinc content [18]. During precipitation synthesis, iron converts more readily to Fe_3O_4, while ZnO forms as a minor phase. This observation is consistent with the qualitative phase estimation obtained from the XRD peak-intensity analysis

described above. In this work, the Fe_3O_4/ZnO composition reflects the intrinsic Fe-Zn ratio present in the CGI waste precursor, which is central to our waste-derived and circular-economy-oriented synthesis strategy. Intentionally modifying this ratio by externally adding Zn^{2+} would shift the process away from a fully waste-derived workflow and introduce non-waste chemical inputs, contradicting the primary objective of valorising CGI waste as the sole metal source. Therefore, the composition reported here represents the natural outcome of the precursor's chemistry rather than an optimised or engineered metal ratio, although such targeted compositional tuning could be a valuable direction for future studies.

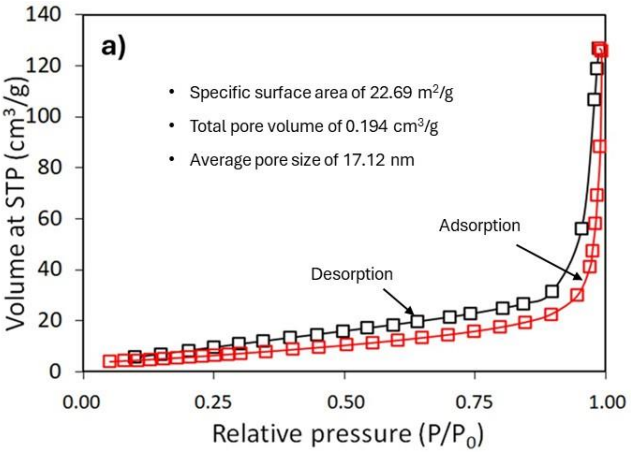

Figure 3. Nitrogen adsorption-desorption isotherm indicating mesoporosity of the synthesised powder

Nitrogen adsorption-desorption analysis evaluated the porous structure of the composite. The results revealed a Brunauer-Emmett-Teller (BET) surface area of 22.7 m^2/g, total pore volume of 0.194 cm^3/g and average pore size of 17.1 nm, classifying it as mesoporous. The nitrogen adsorption-desorption isotherm (Fig. 3) shows typical Type IV(a) behaviour with an H3 hysteresis loop, confirming a mesoporous structure with slit-shaped pores or irregular aggregates, consistent with IUPAC standards [33]. Mesoporosity benefits catalysis by providing many accessible active sites and facilitating reactant diffusion, enhancing reaction efficiency [34,35].

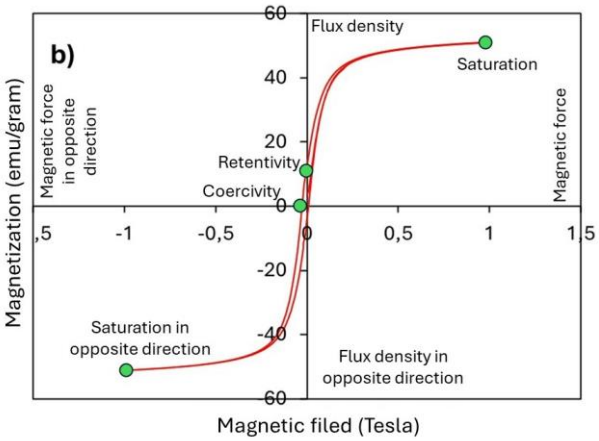

Figure 4. Magnetisation curve showing superparamagnetic behaviour

The magnetization curve (Fig. 4) displays an S-shaped hysteresis loop indicating superparamagnetic behaviour of the Fe_3O_4/ZnO composite with minimal coercivity and remanence [36,37]. The composite's saturation magnetisation is ~51 emu/g, lower than that of pure bulk magnetite (~86 emu/g), likely due to the small Fe_3O_4 particles (the critical size below which Fe_3O_4 particles are paramagnetic is 30 nm) and diamagnetic effect of the minor ZnO phase [38]. The superparamagnetic nature allows easy magnetic separation of the catalyst from solution after reaction, simplifying catalyst recovery and reuse in wastewater treatment [17].

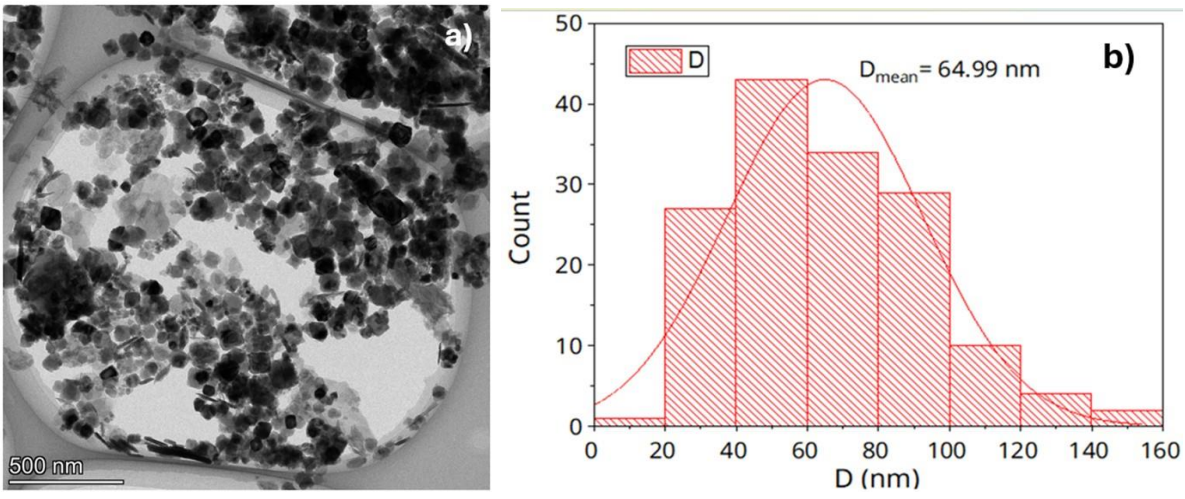

Figure 5. TEM image (a) and particle size distribution histogram (b) of the Fe_3O_4/ZnO composite

TEM analysis (Fig. 5a) provides direct visual evidence of the composite's nanoscale morphology, revealing quasi-spherical, irregular and rod-shaped structures with noticeable agglomeration. This agglomeration aligns with SEM observations and likely results from magnetic dipole and Van der Waals interactions [39]. The particle size distribution histogram (Fig. 5b), derived from measuring over 100 nanoparticles, shows a wide size range with an average diameter of 65.0 nm (20–150 nm). This indicates moderate polydispersity attributable to variations in nucleation and growth during synthesis [40]. A high-resolution TEM image (Fig. 6a) reveals clear lattice fringes, confirming crystalline phases at the nanoscale. Interplanar spacings measure 0.253 nm for Fe_3O_4 (311), 0.493 nm for Fe_3O_4 (111) and 0.248 nm for ZnO (101). These measurements confirm the co-presence of Fe_3O_4 and ZnO phases at the nanometre level, validating the composite formation. The selected area electron diffraction (SAED) pattern (Fig. 6b) confirms the polycrystalline nature, with distinct rings corresponding to Fe_3O_4 (JCPDS No. 19-0629) [41], whereas ZnO is not detected under the HRTEM analysis conditions used in this study. This polycrystalline structure, with observed lattice fringes, robustly supports the XRD-identified crystalline phases and successful component integration.

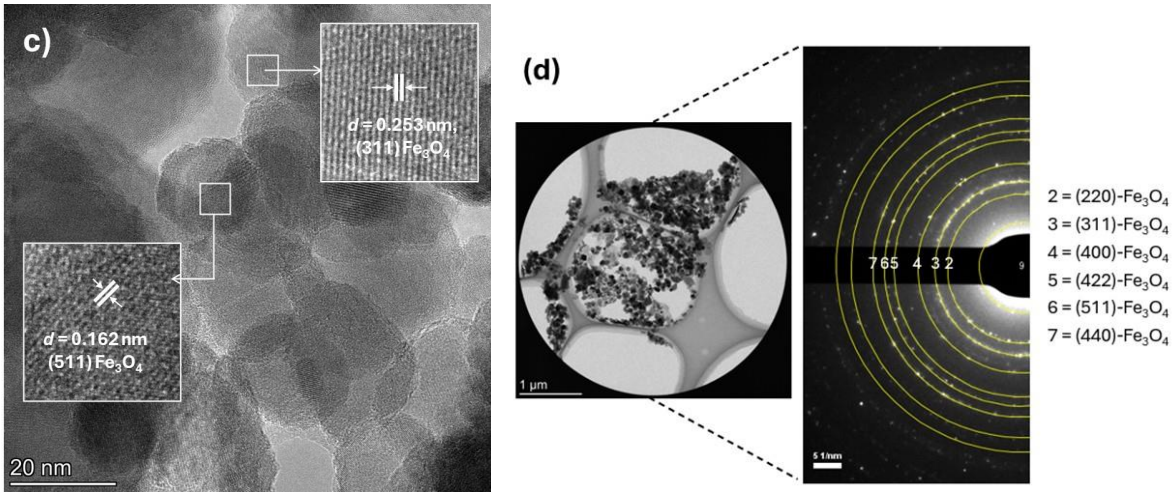

Figure 6. HRTEM image showing lattice fringes corresponding to Fe_3O_4 and ZnO (a), and selected area electron diffraction (SAED) pattern (b) of the Fe_3O_4ZnO composite

XPS provided insights into the surface elemental composition and chemical states, parameters that play a critical role in governing the catalytic performance. The XPS survey spectrum (Fig. 7a) confirms Zn, Fe, O and C, with peaks at Zn 2*p*, Fe 2*p*, O 1*s* and C 1*s* binding energies. The C 1*s* peak at ~284.6 eV arises from adventitious or graphitic carbon [42]. The high-resolution Fe 2*p* spectrum (Fig. 7b) shows peaks at ~710.5 eV (Fe $2p_{3/2}$) and ~724.5 eV (Fe $2p_{1/2}$), with satellite peaks at ~718 and ~732 eV. This pattern, especially the satellites, indicates Fe^{2+} and Fe^{3+} coexistence [43], essential for Fenton redox cycling [44,45]. The high-resolution Zn 2*p* spectrum (Fig. 7c) shows ~1021.8 eV (Zn $2p_{3/2}$) and ~1044.9 eV (Zn $2p_{1/2}$), confirming the presence of Zn^{2+} in the composite powder [46]. The O 1*s* spectrum (Fig. 7d) reveals three components: 529.6 eV (Fe–O in Fe_3O_4), 531.1 eV (Zn–O in ZnO) and 532.7 eV (O–H/adsorbed water) [47]. These XPS results provide surface-sensitive composition and states, complementing bulk XRD and FTIR analyses while confirming Fenton-like active species. Moreover, consistent with the FTIR results, the XPS survey spectrum does not exhibit any N 1*s* peak within the expected binding-energy range of 395–410 eV, confirming the absence of nitrogen-containing species, including nitrate and nitrite, in the final Fe_3O_4/ZnO composite.

In summary, comprehensive characterisation by XRD, FTIR, SEM-EDX, BET, VSM, TEM, HRTEM and XPS consistently confirms successful synthesis of mesoporous, superparamagnetic Fe_3O_4/ZnO composite from CGI waste. These analyses establish Fe_3O_4 and ZnO co-presence at bulk and nanoscale, highlight mixed surface Fe^{2+}/Fe^{3+} states, and confirm excellent magnetic separability. All properties are optimally combined for efficient Fenton-like catalysis.

3.2. Fenton-like catalytic activity evaluation

The Fe_3O_4/ZnO composite demonstrated strong Fenton-like catalytic performance toward methylene blue (MB) degradation, achieving 85.47% removal efficiency within 60 min (Fig. 8a). This result substantially exceeded the 26.60% degradation observed in the absence of catalyst (Fig. 8b), confirming that H_2O_2 alone provides insufficient oxidative capacity for rapid MB decomposition under the experimental conditions employed.

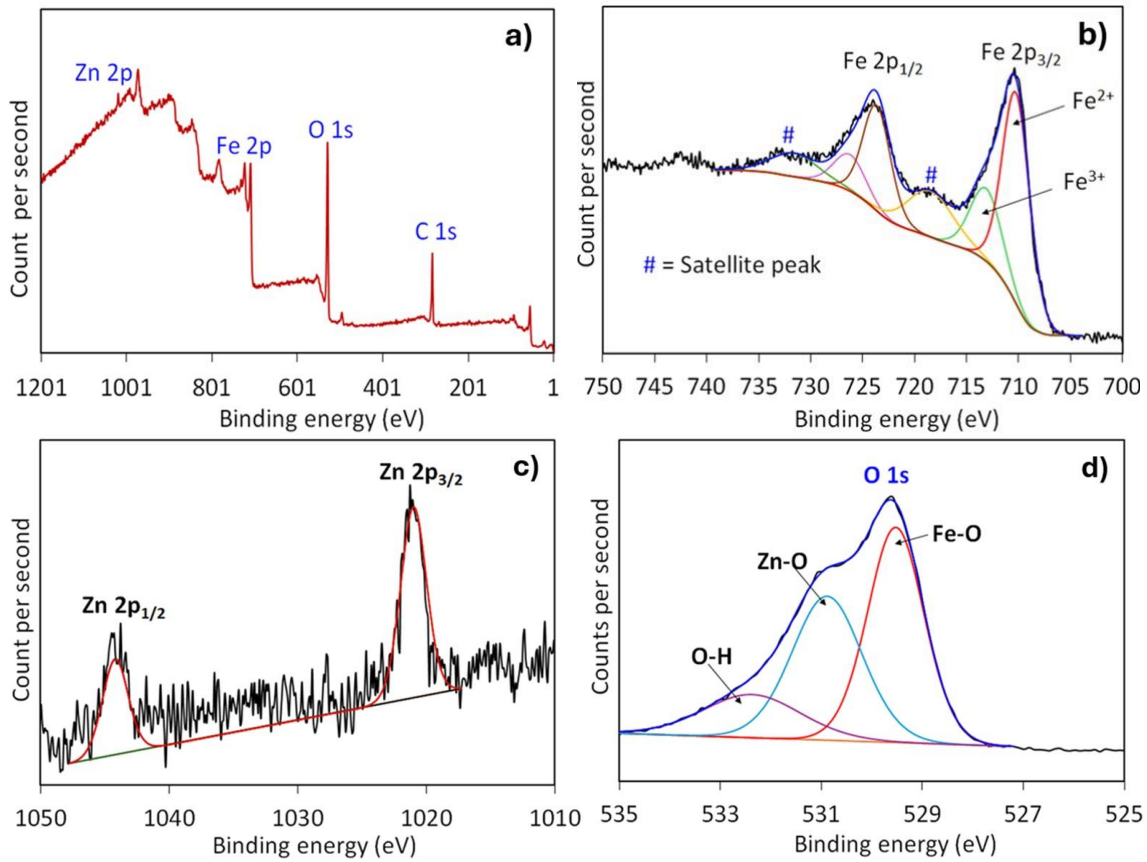

Figure 6. XPS survey spectrum of Fe_3O_4/ZnO composite (a), high-resolution Fe 2*p* spectrum (b), high-resolution Zn 2*p* spectrum (c) and high-resolution O 1*s* spectrum (d)

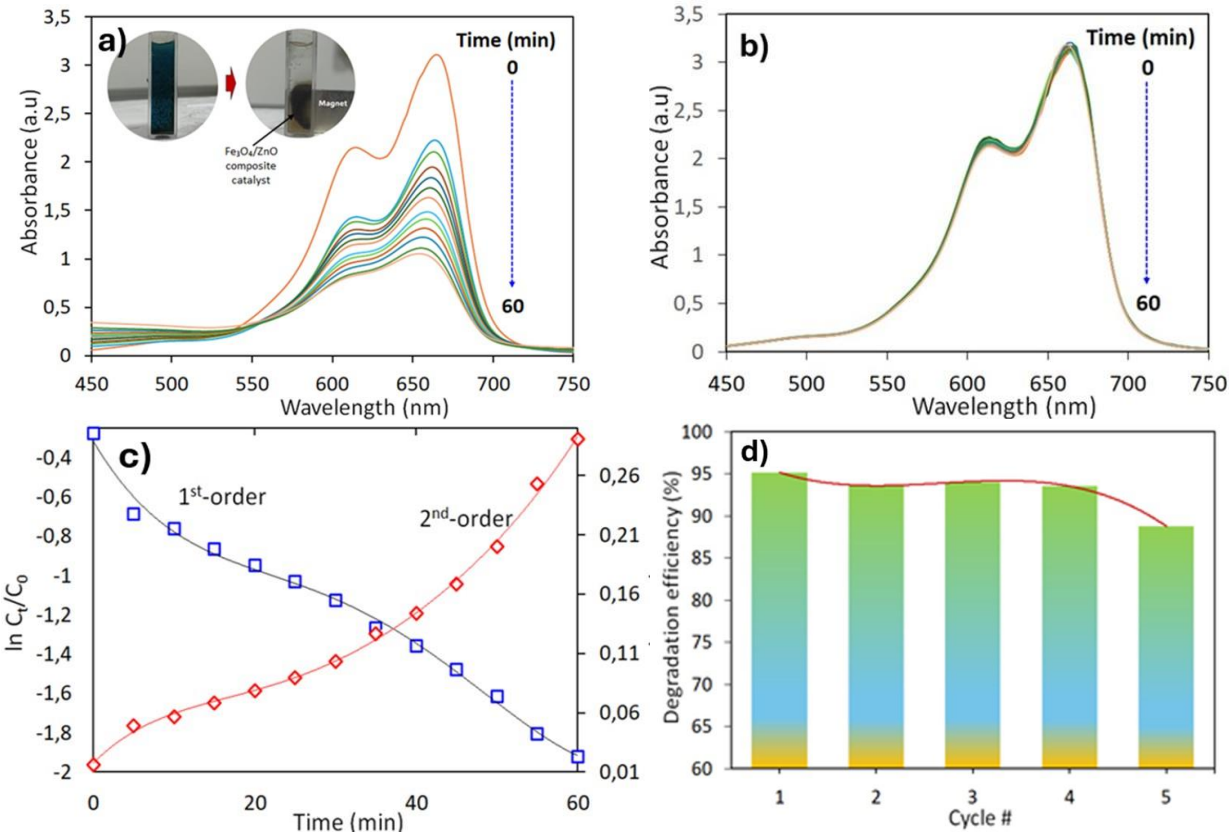

Figure 8. Catalytic degradation of MB using Fe_3O_4/ZnO composite catalyst: a) time-dependent degradation curve, b) control experiment without catalyst, c) kinetic model fitting and d) catalyst recyclability

Beyond its catalytic efficiency, the composite offers a significant practical benefit: it can be easily collected from treated water using a simple magnet due to its superparamagnetic properties (inset of Fig. 8a). This magnetic separation approach is remarkably straightforward [17], the catalyst particles respond rapidly to an external magnetic field and can be removed within seconds. Such ease of recovery eliminates the need for costly filtration systems or energy-consuming centrifugation steps, making the catalyst highly suitable for repeated use in real-world water treatment operations.

Kinetic analysis revealed that MB degradation closely followed first-order reaction kinetics (R^2 = 0.977, rate constant k = 0.024 min^{-1}), substantially outperforming the second-order kinetic model (R^2 = 0.929). This kinetic behaviour aligns well with previous reports describing Fe-based heterogeneous catalysts, including haematite nanocubes [48] and Fe_3O_4@SiO_2 core-shell structures [49], in Fenton-like oxidation reactions.

The enhanced catalytic activity arises from synergistic cooperation between the Fe_3O_4 and ZnO phases. The synergistic role of ZnO within the Fe_3O_4/ZnO composite extends substantially beyond simple physical mixing or additive effects. Previous investigations [48–51] have documented that ZnO enhances charge transfer kinetics and stabilises the Fe^{2+}/Fe^{3+} redox cycle in Fe_3O_4/ZnO composites, thereby accelerating reactive oxygen species generation in heterogeneous Fenton systems. More specifically, the catalytic mechanism operates through the following pathways [44,45,48–51]:

Fe_3O_4 contribution: Fe_3O_4 provides Fe^{2+} active sites that effectively activate H_2O_2 to generate hydroxyl radicals ($^{\bullet}OH$) via the classical Fenton reaction:

- $Fe^{2+} + H_2O_2 \rightarrow Fe^{3+} + {}^{\bullet}OH + OH^-$ (Fenton reaction)
- $Fe^{3+} + H_2O_2 \rightarrow Fe^{2+} + HO_2^{\bullet} + H^+$ (Fe^{3+} reduction)

ZnO contribution: The minor ZnO component facilitates interfacial electron transfer processes and promotes continuous Fe^{2+} regeneration. The Fe_3O_4-ZnO heterojunction enables photoexcited or thermally activated electrons from ZnO to effectively reduce surface-bound Fe^{3+} species back to catalytically active Fe^{2+}, thereby accelerating the regeneration of active sites and sustaining continuous Fenton-like cycling. Furthermore, the intimate interface between Fe_3O_4 and ZnO may create localised electric fields that enhance both H_2O_2 adsorption and subsequent activation, further amplifying $^{\bullet}OH$ production. This mechanistic synergy-effectively combining Fe-based redox activity with ZnO-mediated electron facilitation-provides a compelling explanation for the superior catalytic activity observed in this work relative to standalone Fe_3O_4 materials or simple physical mixtures.

The predominant degradation pathway proceeds through $^{\bullet}OH$ generation via the classical Fe^{2+}/Fe^{3+} redox cycling mechanism, consistent with mechanistic frameworks established in prior Fe_3O_4/ZnO catalytic studies. Although direct spectroscopic detection of $^{\bullet}OH$ radicals via electron paramagnetic resonance (EPR) spectroscopy was not performed in the current investigation, the proposed hydroxyl radical-mediated mechanism receives strong indirect support from multiple lines of evidence: i) the experimentally observed Fe^{2+}/Fe^{3+} mixed-valence states confirmed through XRD analysis and magnetisation measurements, ii) the characteristic first-order degradation kinetics that typify $^{\bullet}OH$-driven oxidation processes and iii) extensive mechanistic precedent established throughout the Fenton-like catalysis literature for Fe_3O_4-based heterogeneous systems operating under comparable reaction conditions.

Similar mechanistic interpretations relying on integrated redox evidence and kinetic modelling approaches have been extensively validated across numerous prior investigations of heterogeneous Fenton catalysts [8,44,45,48,52,53]. Nevertheless, direct spectroscopic confirmation of reactive oxygen species using EPR techniques will be systematically pursued in forthcoming work to provide unambiguous experimental validation of the $^{\bullet}OH$ generation pathway and to rigorously quantify the relative contributions of $^{\bullet}OH$, superoxide ($O_2^{\bullet-}$), and other transient radical species to the overall pollutant degradation mechanism.

Table 1. Comparative performance of Fe_3O_4-based catalysts for MB degradation under dark Fenton-like conditions, highlighting the CGI waste-derived Fe_3O_4/ZnO catalyst

Catalyst composition	Synthesis method	Reaction conditions (H_2O_2 conc., pH, catalyst dose, temperature)	Time [min]	MB Removal [%]	Ref.
Fe_3O_4/ZnO (CGI waste-derived)	Co-precipitation method	15 mM, pH ~5, 0.5 g/l, ~25 °C	60	85.47	This study
Fe_3O_4/ montmorillonite	Co-precipitation method	~200 mM, pH 3, 0.5 g/l, ~20 °C	120	90	[8]
Fe_3O_4 nanoparticles	Hydrothermal method	0.32 mM, pH 4.8, 0.6 g/l, not specified	20	~100	[54]
Fe_3O_4@C	*In situ*, solid-phase reaction	30 mM, pH 5, 2 g/l, 25 °C	275	~99	[55]

To properly contextualise the catalytic performance achieved in this study, a systematic benchmarking comparison with previously reported Fe_3O_4-based catalysts operating under dark Fenton-like conditions was conducted. As summarised in Table 1, the CGI waste-derived Fe_3O_4/ZnO catalyst achieves 85.47% methylene blue removal at only 15 mM H_2O_2, pH ~5, and a catalyst dose of 0.5 g/l within 60 min, which is comparable to or better than other systems that typically require more acidic conditions, higher oxidant dosages, longer reaction times, or higher catalyst loadings to reach similar degradation efficiencies. Notably, the high catalytic activity achieved under mild reaction conditions-specifically without UV irradiation assistance or externally supplemented Zn^{2+} sources, strongly highlights both the practicality and resource-efficient nature of the present waste-derived catalyst synthesis strategy.

Catalyst reusability tests (Fig. 8d) demonstrated excellent operational stability, with the Fe_3O_4/ZnO composite maintaining degradation efficiency exceeding 93.58% over four consecutive reaction cycles, declining only marginally to 88.76% in the fifth cycle. This slight performance reduction likely originates from a combination of factors including minor catalyst mass loss during magnetic separation and washing steps, progressive surface fouling by organic degradation intermediates, partial deactivation of surface-active sites, or gradual leaching of catalytically active Fe and Zn ionic species-phenomena commonly reported for Fe-based heterogeneous Fenton catalysts operating under oxidative conditions [48,49]. Despite this modest decline, the results convincingly confirm both the structural robustness and practical regenerative potential of this CGI waste-derived catalytic material, thereby supporting its viability for economically sustainable, multi-cycle wastewater treatment applications.

3.3. Future directions

This study shows that CGI waste can be directly converted into a functional Fe_3O_4/ZnO composite powder with promising Fenton-like activity, but several important aspects still require deeper investigation to strengthen both the mechanistic insight and practical relevance of this approach. Because the Fe_3O_4/ZnO ratio used here follows the natural Fe-Zn composition of the CGI waste, the process remains simple, fully waste-derived and free from additional chemical inputs. Although adding external Zn^{2+} could potentially enhance performance, this work intentionally prioritises a low-cost and realistic route. Moving forward, controlled tuning of the composition will be important for clarifying structure-activity relationships and identifying the most effective ratio. Moreover, direct reactive oxygen species detection using EPR, together with post-reaction XPS to track Fe^{2+}/Fe^{3+} surface changes, will be essential for resolving the reaction mechanism, while Rietveld refinement can provide stronger support than the current qualitative XRD assessment. It will also be necessary to verify whether nitrogen residues from the HNO_3 dissolution step remain in the product using ion chromatography or elemental analysis to ensure catalyst purity and environmental safety. From an application perspective, evaluating the catalyst against a broader range of pollutants, including pharmaceuticals, persistent organics and real wastewater, alongside long-term stability and leaching tests using ICP-MS and pathway analysis via GC-MS or LC-MS, will help establish its robustness. Ultimately, developing scalable synthesis protocols supported by techno-economic and life-cycle assessments will be crucial for determining whether this waste-to-catalyst approach is viable for larger-scale environmental remediation.

IV. Conclusions

This study demonstrates a sustainable strategy to valorise CGI waste by converting it into a mesoporous and superparamagnetic Fe_3O_4/ZnO composite particles, exhibiting effective Fenton-like catalytic activity for methylene blue (MB) degradation. The novelty lies in transforming an abundant industrial residue into a functional composite through a simple and efficient route, achieving notable catalytic performance without external irradiation or complex activation steps. The synergistic combination of Fe_3O_4 and ZnO imparts high surface area, well-defined mesoporosity and efficient magnetic recovery, positioning the material as a promising candidate for wastewater treatment. The catalytic behaviour is driven by synergistic Fe^{2+}/Fe^{3+} redox cycling, the porous architecture that enhances mass transfer and the intimate Fe_3O_4-ZnO interface, collectively promoting reactive oxygen species generation and improving pollutant accessibility. Its superparamagnetic nature further enables facile post-reaction separation, supporting repeated catalytic cycles. Overall, this work provides a straightforward and sustainable pathway for converting CGI waste into a functional Fe_3O_4/ZnO composite while elucidating key mechanistic insights, offering guidance for future development of waste-derived catalysts and scalable applications.

Acknowledgement: The authors appreciate ELSA-BRIN for characterisation support and Research Centre for Molecular Chemistry-BRIN for laboratory access.

References

1. H. Abera, C.A. Elmer, D. Mamaru, "Comparative Analysis on Roof Covering Materials Sustainability as Constructed by Bamboo and Corrugated Galvanized Iron Sheet in Rural Areas Around Wolkite, Ethiopia", *Int. J. Sustain. Constr. Eng. Technol.*, **13** (2022) 147–158.
2. A.P.M. Velenturf, P. Purnell, "Principles for a sustainable circular economy", *Sustain. Prod. Consum.*, **27** (2021) 1437–1457.
3. J.-M. Gao, S. Ma, Z. Du, F. Cheng, P. Li, "Zinc-bearing dust derived non-toxic mixed iron oxides as magnetically recyclable photo-Fenton catalyst for degradation of dye", *Water Sci. Technol*., **83** (2020) 425–434.
4. B. Wareppam, N.J. Singh, S. Chakraborty, N. Aomoa, M. Kakati, A.C. de Oliveira, V.K. Garg, K.P. Singh, S. Barg, S. Ghosh, L.H. Singh, "Unused to useful: Recycling plasma chamber coated waste composite of ZnO and α-Fe_2O_3 into an active material for sustainable waste-water treatment", *Chem. Eng. J. Adv*., **7** (2021) 100120.
5. C. Wang, R. Jiang, J. Yang, P. Wang, "Enhanced heterogeneous Fenton degradation of organic pollutants by CRC/Fe_3O_4 catalyst at neutral pH", *Front. Chem*., **10** (2022) 892424.
6. W. Wang, Q. Mao, H. He, M. Zhou, "Fe_3O_4 nanoparticles as an efficient heterogeneous Fenton catalyst for phenol removal at relatively wide pH values", *Water Sci. Technol*., **68** (2013) 2367–2373.
7. S.-T. Yang, W. Zhang, J. Xie, R. Liao, X. Zhang, B. Yu, R. Wu, X. Liu, H. Li, Z. Guo, "Fe_3O_4@SiO_2 nanoparticles as a high-performance Fenton-like catalyst in a neutral environment", *RSC Adv*., **5** (2015) 5458–5463.
8. H. Ayadi, A. Khaled, S. Halladja, I. Boudraa, Z. Rehimi, M.M. Chehimi, "Fe_3O_4/MMT Fenton-like heterogeneous catalyst for the methylene blue degradation", *Desalin. Water Treat*., **260** (2022) 179–186.
9. P. Chhattise, S. Saleh, V. Pandit, S. Arbuj, V. Chabukswar, "ZnO nanostructures: a heterogeneous catalyst for the synthesis of benzoxanthene and pyranopyrazole scaffolds via a multi-component reaction strategy", *Mater. Adv*., **1** (2020) 2339–2345.
10. A. Zehra Yiğit, İ. Duru, E. Sayan, "Improved photocatalytic degradation of methylene blue by novel hexagonal ZnO particles", *Water SA*, **50** (2024) 392−403.
11. H. Neelamkodan, U. Megha, M. Chennabasappa, M.P. Binitha, "Bicone nanoflower evolution and multi-peak emission of polymer caped Cu doped ZnO", *Nanotechnology*, **35** (2024) 355701.
12. H. Neelamkodan, U. Megha, M.P. Binitha, "Multi peak emission and morphological evolution of Fe-doped ZnO nanoflowers", *Process. Appl. Ceram*., **17** (2023) 149–156.
13. H. Neelamkodan, U. Megha, M.P. Binitha, "Enhanced green luminescence properties of cu doped ZnO nano-flowers and their improved antibacterial", *Process. Appl. Ceram.*, **17** [1] (2023) 81–90.
14. A. McLaren, T. Valdes-Solis, G. Li, S.C. Tsang, "Shape and size effects of ZnO nanocrystals on photocatalytic activity", *J. Am. Chem. Soc*., **131** (2009) 12540–12541.
15. P. Chen, Y. Zhao, C. Li, X. Chen, J. Wang, "Interfacial engineering of Fe-O-Zn bonds in heterojunction photocatalysts: synergistic visible light PMS activation and electron transfer efficiency enhancement", *J. Mater. Chem. A*, **13** (2025) 25829–25841.
16. G. Ren, K. Zhao, L. Zhao, "A Fenton-like method using ZnO doped MIL-88A for degradation of methylene blue dyes", *RSC Adv*., **10** (2020) 39973–39980.
17. S.M. Devi, A. Nivetha, I. Prabha, "Superparamagnetic properties and significant applications of iron oxide nanoparticles for astonishing efficacy - A review", *J. Supercond. Novel Magn.*, **32** (2019) 127–144.
18. C. Shi, Y. Huang, S. Su, G. Han, H. Sun, S. Yang, B. Liu, "Ultrafast recovery of Zn from waste galvanized iron sheet by ultrasound-assisted acid pickling and ion flotation techniques", *Ultrason. Sonochem.*, **114** (2025) 107237.
19. Y. Bing, C. Ding, "Synthesis of CuO nanoparticles for catalytic application via ultrasound-assisted ball milling", *Process. Appl. Ceram*., **11** (2017) 39–44.
20. A. Ahmad, P.G. Roy, A. Hassan, S. Zhou, M. Azam, M.A.Z.G. Sial, A. Irfan, F. Kanwal, R. Begum, Z.H. Farooqi, "Catalytic degradation of various dyes using silver nanoparticles fabricated within chitosan based microgels", *Int. J. Biol. Macromol*., **283** (2024) 137965.
21. O. Zuas, F.A. Dzakirah, T. Sudiro, "Harnessing Sterculia Foetida seed coat for silver nanoparticles biofabrication: Characterization and a rapid, highly efficient catalyst for methylene blue degradation", *Biointerface Res. Appl. Chem*., **15** (2025) 38.
22. V. Alfredo Reyes Villegas, J. Isaías De León Ramírez, E. Hernandez Guevara, S. Perez Sicairos, L. Angelica Hurtado Ayala, B. Landeros Sanchez, "Synthesis and characterization of magnetite nanoparticles for photocatalysis of nitrobenzene", J. *Saudi Chem. Soc.*, **24** (2020) 223–235.
23. S. Jayswal, R.S. Moirangthem, "Thermal decomposition route to synthesize ZnO nanoparticles for photocatalytic application", *AIP Conf. Proc*., **2009** (2018) 020023.
24. M. Ma, Y. Zhang, W. Yu, H.-y. Shen, H.-Q. Zhang, N. Gu, "Preparation and characterization of magnetite nanoparticles coated by amino silane", *Colloids Surf. A Physicochem. Eng. Asp*., **212** (2003) 219–226.
25. M. Neamtu, C. Nadejde, L. Brinza, O. Dragos, D. Gherghel, A. Paul, "Iron phthalocyanine-sensitized magnetic catalysts for BPA photodegradation", *Sci. Rep.*, **10** (2020) 5376.
26. S. Dutta, B.N. Ganguly, "Characterization of ZnO nanoparticles grown in presence of Folic acid template", *J. Nanobiotechnol*., **10** (2012) 29.
27. F.A. Miller, C.H. Wilkins, "Infrared spectra and characteristic frequencies of inorganic ions", *Anal. Chem*., **24** (1952) 1253–1294.
28. K. Al-Amin, M. Kawsar, M.T.R.B. Mamun, M. Sahadat Hossain, "Fourier transform infrared spectroscopic technique for analysis of inorganic materials: a review", *Nanoscale Adv*., **7** (2025) 6677–6702.
29. M.H. Brooker, D.E. Irish, "Infrared and Raman spectroscopic studies of solid alkali metal nitrites", *Can. J. Chem*., **49** (1971) 1289–1295.
30. M. Nayan, J. Krishnegowda, M. Abhilash, D.N. Keerthiraj, S. Shivanna, "Comparative study on the effects of surface area, conduction band and valence band positions on the photocatalytic activity of ZnO-M_xO_y heterostructures", *J. Water Resour. Prot*., **11** (2019) 357–370.

31. Y. Cherifi, A. Chaouchi, Y. Lorgoilloux, M. Rguiti, A. Kadri, C. Courtois, "Electrical, dielectric and photocatalytic properties of Fe-doped ZnO nanomaterials synthesized by sol gel method", *Process. Appl. Ceram*., **10** (2016) 125–135.
32. Y. Cao, C. Li, J. Li, Q. Li, J. Yang, "Magnetically separable Fe_3O_4/AgBr hybrid materials: Highly efficient photocatalytic activity and good stability", *Nanoscale Res. Lett*., **10** (2015) 251.
33. M. Thommes, K. Kaneko, A.V. Neimark, J.P. Olivier, F. Rodriguez-Reinoso, J. Rouquerol, K.S.W. Sing, "Physisorption of gases, with special reference to the evaluation of surface area and pore size distribution (IUPAC Technical Report)", *Pure Appl. Chem*., **87** (2015) 1051–1069.
34. J.A. Cecilia, R. Moreno Tost, M. Retuerto Millán, "Mesoporous materials: From synthesis to applications", *Int. J. Mol. Sci*., **20** [13] (2019) 3213.
35. J. Lantos, N. Kumar, B. Saha, "A comprehensive review of fine chemical production using metal-modified and acidic microporous and mesoporous catalytic materials", *Catalysts*, **14** [5] (2024) 317.
36. J. Wan, H. Li, K. Chen, "Synthesis and characterization of Fe_3O_4@ZnO core–shell structured nanoparticles", *Mater. Chem. Phys.*, **114** (2009) 30–32.
37. Y.-H. Zheng, Y. Cheng, F. Bao, Y.-S. Wang, "Synthesis and magnetic properties of Fe_3O_4 nanoparticles", *Mater. Res. Bull*., **4**1 (2006) 525–529.
38. R.A. da Silva, M.J. Jacinto, V.C. Silva, D.C. Cabana, "Urea-assisted fabrication of Fe_3O_4@ZnO@Au composites for the catalytic photodegradation of Rhodamine-B", *J. Sol-Gel Sci. Technol*., **86** (2018) 94–103.
39. C. Appel, B. Kuttich, T. Kraus, B. Stühn, "In situ investigation of temperature induced agglomeration in non-polar magnetic nanoparticle dispersions by small angle X-ray scattering", *Nanoscale*, **13** (2021) 6916–6920.
40. S. Laurent, D. Forge, M. Port, A. Roch, C. Robic, L. Vander Elst, R.N. Muller, "Magnetic iron oxide nanoparticles: Synthesis, stabilization, vectorization, physicochemical characterizations, and biological applications", *Chem. Rev*., **108** (2008) 2064–2110.
41. P. Hu, L. Kang, T. Chang, F. Yang, H. Wang, Y. Zhang, J. Yang, K.-S. Wang, J. Du, Z. Yang, "High saturation magnetization Fe_3O_4 nanoparticles prepared by one-step reduction method in autoclave", *J. Alloys Compd*., **728** (2017) 88–92.
42. A.P. Dementjev, A. de Graaf, M.C.M. van de Sanden, K.I. Maslakov, A.V. Naumkin, A.A. Serov, "X-ray photoelectron spectroscopy reference data for identification of the C_3N_4 phase in carbon–nitrogen films", *Diamond Relat. Mater*., **9** (2000) 1904–1907.
43. I.N. Reddy, A. Sreedhar, C.V. Reddy, J. Shim, M. Cho, D. Kim, J.S. Gwag, K. Yoo, "Enhanced visible-light photocatalytic performance of Fe_3O_4 nanopyramids for water splitting and dye degradation", *J. Solid State Electrochem*., **22** (2018) 3535–3546.
44. C. Lai, X. Shi, L. Li, M. Cheng, X. Liu, S. Liu, B. Li, H. Yi, L. Qin, M. Zhang, N. An, "Enhancing iron redox cycling for promoting heterogeneous Fenton performance: A review", *Sci. Total Environ*., **775** (2021) 145850.
45. Y. Liu, J. Wang, "Multivalent metal catalysts in Fenton/Fenton-like oxidation system: A critical review", *Chem. Eng. J*., **466** (2023) 143147.
46. M. Roeinfard, A. Bahari, "Nanostructural characterization of the Fe_3O_4/ZnO magnetic nanocomposite as an application in medicine", *J. Supercond. Novel Magn.*, **30** (2017) 3541–3548.
47. L. Qi, S. Wang, Y. Liu, P. Zhao, J. Tian, B. Zhu, S. Zhang, W. Xie, H. Yu, "Facile preparation of magnetically separable Fe_3O_4/ZnO nanocomposite with enhanced photocatalytic activity for degradation of Rhodamine B", *Nanomaterials*, **14** [11] (2024) 926.
48. D. Das, S. Ali, B. Rajbanshi, S. Ray, S. Barman, D. Chouhan, M.S. Haydar, P. Mandal, K. Roy, V.K. Dakua, M. Nath Roy, "Synthesis of biogenic hematite nanocubes as recyclable dark Fenton-like catalysts at neutral pH and plant growth applications of degraded waste water", *ACS Omega*, **7** (2022) 44698–44710.
49. N. Mahmud, A. Benamor, M.S. Nasser, M.M. Ba-Abbad, M.H. El-Naas, A.W. Mohammad, "Effective heterogeneous Fenton-like degradation of malachite green dye using the core-chell Fe_3O_4@SiO_2 nano-catalyst", *ChemistrySelect*, **6** (2021) 865–875.
50. P.-J. Lin, C.-H. Yeh, J.-C. Jiang, "Theoretical insight into hydroxyl production via H_2O_2 decomposition over the Fe_3O_4(311) surface", *RSC Adv*., **11** (2021) 36257–36264.
51. S. Song, Y. Wang, H. Shen, J. Zhang, H. Mo, J. Xie, N. Zhou, J. Shen, "Ultrasmall graphene oxide modified with Fe_3O_4 nanoparticles as a Fenton-like agent for methylene blue degradation", *ACS Appl. Nano Mater*., **2** (2019) 7074–7084.
52. A. Gogoi, M. Navgire, K.C. Sarma, P. Gogoi, "Fe_3O_4-CeO_2 metal oxide nanocomposite as a Fenton-like heterogeneous catalyst for degradation of catechol", *Chem. Eng. J.*, **311** (2017) 153–162.
53. X. Liu, Y. Yao, J. Lu, J. Zhou, Q. Chen, "Catalytic activity and mechanism of typical iron-based catalysts for Fenton-like oxidation", *Chemosphere*, **311** (2023) 136972.
54. A. Khorshidi, A. Fallah Shojaei, S. Shariati, R. Amin, "Efficient Fenton like degradation of methylene blue in aqueous solution by using Fe_3O_4 nanoparticles as catalyst", *Chem. Solid Mater*., **2** (2014) 17–23.
55. H. Xiang, G. Ren, Y. Zhong, D. Xu, Z. Zhang, X. Wang, X. Yang, "Fe_3O_4@C nanoparticles synthesized by in situ solid-phase method for removal of methylene blue", *Nanomaterials*, **11** (2021) 330.